Journal Name

ARTICLE TYPE

Cite this: DOI: 10.1039/xxxxxxxxxx

Nanoparticle-Polymer Interfacial Layer Properties Tunes Fragility and Dynamic Heterogeneity of Athermal Polymer Nanocomposite films

Nafisa Begam [a†], Nimmi Das A [a], Sivasurender Chandran [b], Mohd Ibrahim [a], Venkat Padmanabhan [c], Michael Sprung [d], and J. K. Basu[a*]

Received Date
Accepted Date

DOI: 10.1039/xxxxxxxxxx

www.rsc.org/journalname

Enthalpic interactions at the interface between nanoparticles and matrix polymers is known to influence various properties of the resultant polymer nanocomposites (PNC). For athermal PNCs, consisting of grafted nanoparticles embedded in chemically identical polymers, the role and extent of the interface layer (IL) interactions in determining the properties of the nanocomposites is not very clear. Here, we demonstrate the influence of the interfacial layer dynamics on the fragility and dynamical heterogeneity (DH) of athermal and glassy PNCs. The IL properties are altered by changing the grafted to matrix polymer size ratio, f , which in turn changes the extent of matrix chain penetration into the grafted layer, λ. The fragility of PNCs is found to increase monotonically with increasing entropic compatibility, characterised by increasing λ. Contrary to observations in most polymers and glass formers, we observe an anti-correlation between the dependence on IL dynamics of fragility and DH, quantified by the experimentally estimated Kohlrausch-Watts-Williams parameter and the non-Gaussian parameter obtained from simulations.

1 Introduction

The nature of nanoparticle (NP)-polymer interface plays a crucial role in determining flow, thermal, mechanical, optical and electrical properties[1–5] of polymer nanocomposites (PNC). Almost a decade back we had shown, for the first time, how glass transition temperature, T_g, can be tuned by controlling the nature of NP-polymer interfacial layer (IL) and confinement of polymer chains due to NPs in athermal PNCs[6]. Recently, there has been renewed interest in correlating several other properties of PNCs in terms of the structure and dynamics of IL especially for enthalpic PNCs[7–10]. A fundamental difference between the IL in enthalpic and entropic PNCs, often based on polymer grafted nanoparticles (PGNP), used by us and others[11–15] is in their nature and formation. While the width and structure of the IL for enthalpic PNCs[16] is largely determined by the strength of the NP-polymer segmental interactions and the molecular weight of the matrix polymer[7,8], for PGNP based entropic PNCs this is dependent on the ratio of the grafted and matrix polymer molecular weight, f, grafting density and NP size among other parameters[11,12,17]. More importantly, f, also determines the effective entropic interaction between the PGNPs turning from attractive at low f to repulsive at larger f, which also allows control over the state of dispersion of PNCs ultimately determining the efficacy of these materials. At a more fundamental level the matrix chain penetration depth, λ, is directly proportional to f and can be defined as the microscopic parameter, which controls the extent of entropic interaction[18]. The concept of fragility, m, has proven to be useful in understanding the diversity of dynamics seen in various glass formers, including polymers[19,20]. Some understanding has emerged to explain the differences in the fragilities and its relation with various thermodynamic properties, physical aging, and mechanical behavior[21,22], while for soft colloidal glass formers it has been shown that fragility can be tuned by varying the strength of the inter-particle interactions[23].

In enthalpy dominated PNCs the fragility was shown to increase with the inclusion of particles with attractive interactions with the matrix polymers, while the particles with repulsive interactions show a decrease in the fragility[24]. It has been shown recently, that apart from T_g and viscosity, fragility in enthalpic PNCs can be tuned by changing the structure of the IL[7,8,10,24,25]. However, for entropic PNCs it was suggested that fragility remains largely unaltered due to inclusion of NPs[26].

Another key dynamical parameter, which has been widely used

[a] Department of Physics, Indian Institute of Science, Bangalore, 560012, India ; E-mail: basu@iisc.ac.in
[b] Institute of Physics, University of Freiburg, 79104 Freiburg, Germany
[c] Department of Chemical Engineering, Tennessee Technological University, Cookeville, TN 38505, USA
[d] Deutsches Elektronen Synchrotron DESY, Notkestresse 85, 22607 Hamburg, Germany
† Current Address: Institut für Angewandte Physik, Universität Tübingen, 72076 Tübingen, Germany

Table 1 Sample details

Sample	W_m kDa	W_g kDa	f	$2*R_{pgnp}$ nm	R_g nm
PS50k	50	-	0.0		5.9
3k50k	50	3	0.06	6	
20k50k	50	20	0.4	8.5	
PS100k	100	-	0.0		8.45
3k100k	100	3	0.03	6	
20k100k	100	20	0.2	8.5	

W_m and W_g are the molecular weight of matrix and grafted chains, respectively; R_{pgnp} is the radius of nanoparticle determined from small angle X-ray scattering (Fig. S1[32]); R_g is the radius of gyration of matrix chains. Grafting densities of 3k and 20k grafted nano particles are 1.7 and 1.3 chains/nm^2, respectively.

to describe glasses and supercooled liquids, including polymers and PNCs, is dynamic heterogeneity (DH)[27–29]. In the case of enthalpic PNCs, m seems to correlate with DH (increases for attractive and decreases for repulsive interactions) quantified in terms of a temperature dependent dynamical length scale, ξ, which seems to grow moderately on approaching the glass transition temperature[7,24,29,30]. On the other hand some studies suggest that DH decreases with increasing fragility[31] in amorphous polymers. Surprisingly, very little is known in terms of fragility, DH or their correlations for entropic PNCs[6,26,28].

In this report, we study the temperature dependent relaxation dynamics of typical entropic PNCs consisting of polystyrene grafted gold nanoparticles dispersed in polystyrene (PS) films. Using X-ray photon correlation spectroscopy (XPCS), we extract temperature dependent viscosity, η, of various PNC films as a function of f and estimate their respective fragilities, m. We find that in these PNCs m increases with increasing f, which is also corroborated, qualitatively, by coarse grained molecular dynamics (MD) simulations on similar systems. The experimentally extracted Kohlrausch-Watts-Williams (KWW) parameter, β, is a typical parameter used to quantify DH. β (DH) was found to increase (decrease) with increasing f. Coupled with this, the non-Gaussian parameter (NGP) and interface chain diffusivity was found to decrease with increasing f suggesting a correlation between DH and IL dynamics. However, the variation of m and T_g with f showed an anti-correlation compared with the variation of DH with f, contrary to several earlier studies on glasses and PNCs.

2 Experimental details

The results presented in this letter are based on thin films (thickness, $h \approx$ 65-70 nm; Table S2[32]) of PS of two different molecular weights (100 kDa and 50 kDa), embedded with PGNPs having two different grafted chain molecular weights (3 kDa and 20 kDa) synthesized using methods discussed earlier[33–35]. These PGNPs were dispersed in linear PS at 0.5% volume fraction of the gold core. Details of samples are provided in the supplemental information (SI)[32] as well as in our earlier studies[33,34] and summarized in Table 1.

X-ray photon correlation spectroscopy measurements[36–38] were performed on the annealed PNC films in grazing incidence geometry at PETRA III (beamline P10), DESY, Hamburg, Germany. The measurements were done with an X-ray beam of energy 8 keV and beam size 25×25 μm^2. The beam was incident on the sample at an angle θ, chosen to be smaller than the critical angle of the films[15] for that particular X-ray energy. The critical angle was estimated as the position of first minima of the X-ray reflectivity profile which appears before the substrate critical angle[39]. Typically, the PNC films critical angle was found to be around $\sim 0.16^\circ$. The scattered intensity from the samples were collected by a CCD detector (Lambda, area 1536×512 px^2 (84.5×28.2 mm^2), pixel size of 55×55 μm^2) as a reciprocal image. A typical CCD image of such scattering is shown in Fig. S6[32]. The measurements were performed at the temperatures varying from 403K to 463K. To obtain the intensity autocorrelation function, $g_2(q_x,t)$, typically, 2000 images were collected with an interval of 0.4 sec at each temperature for all the samples. From these image series, we have extracted $g_2(q_x,t)$ and modeled them by a function of the following form[40–42]

$$g_2(q_x,t) = 1 + b|F(q_x,t)|^2, \tag{1}$$

where, the intermediate scattering function (ISF) is given by

$$F(q_x,t) = e^{-(\Gamma\cdot t)^\beta}, \tag{2}$$

where b is an instrumental factor called the speckle contrast, t is delay time, $\Gamma = 1/\tau$ is the relaxation rate, τ is the relaxation time and β, the Kohlrausch exponent, is a canonical gauge for quantifying the deviation in the relaxation behavior from simple exponential.

We can see from Fig. 2 that Γ follows the power law of q_x with an exponent 4 but not 2 which suggests the validation of hydrodynamic continuum theory (HCT)[42–44]. Therefore, the wave vector dependence of relaxation rate is modeled using HCT and relaxation rate is given by[15,45]

$$\Gamma(q_x) = \frac{1}{\tau(q_x)} = \frac{\gamma}{2\eta}\frac{q_x(sinh(q_xh)cosh(q_xh) - (q_xh))}{cosh^2(q_xh) + (q_xh)^2}. \tag{3}$$

Here, η and γ denotes the viscosity and surface tension of the film, h and q_x are thickness of the film and in-plane wave vector respectively.

The viscosity of the films show temperature dependence which is modeled using the well known Vogel-Fulcher-Tammann (VFT) equation[46],

$$\eta = \eta_o \exp\left(\frac{BT_o}{T - T_o}\right), \tag{4}$$

where η_o and B are the fit parameters, T is absolute temperature and T_0 is VFT temperature[32].

Using the temperature dependence of viscosity as obtained from eqn. 4, the fragility, m, can be estimated[32,47] using the definition,

$$m = \left.\frac{\partial log\eta}{\partial\left(\frac{T_g}{T}\right)}\right|_{T_g} \tag{5}$$

where T_g is the glass transition temperature of the films.

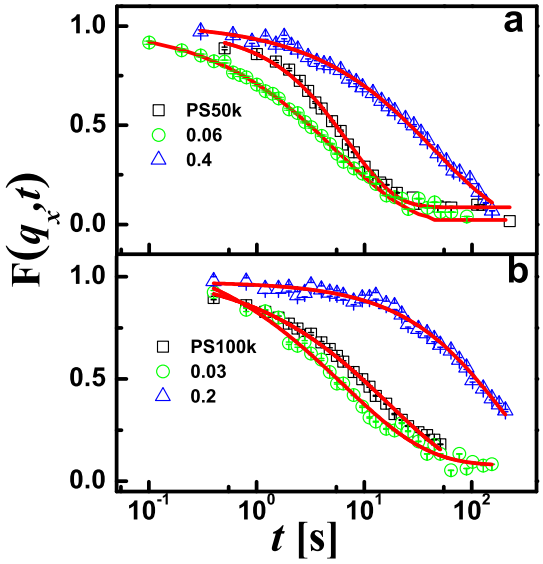

Fig. 1 Representative ISF (a) for pure PS50k and corresponding composites with f = 0.06 and f = 0.4 samples and (b) for pure PS100k, f = 0.03 and f = 0.2 as indicated in respective panels. All the correlation functions were obtained at temperature 433 K and the lateral wave-vector $q_x = 7 \times 10^{-4}$ Å^{-1}. The solid red lines are the fit to the eqn 2.

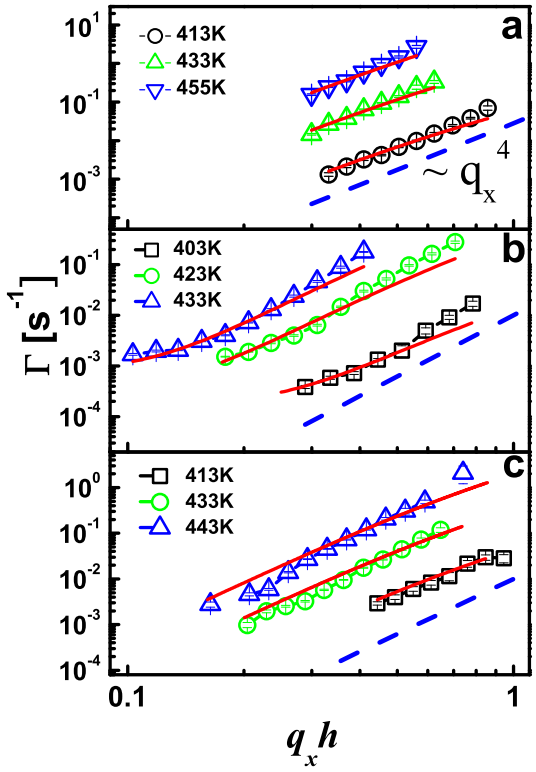

Fig. 2 Wave vector (q_x) dependent relaxation rate Γ as a function of $q_x h$ for (a) f = 0, (b) 0.06 and (c) 0.4 at different temperatures (c). The red lines are the fits to the eqn 3. The dashed line represents the power law q_x^4.

3 Results

Figure 1(a) shows representative ISFs, $F(q_x,t)$, collected from XPCS measurements for PS50k based PNCs at 433 K (Fig. S8[32]). In comparison with neat polymer, a faster dynamics can be observed for 3k50k ($f = 0.06$) sample, while 20k50k ($f = 0.4$) sample shows a slower dynamics. Similar behavior can be observed for PS100k based samples as shown in Fig. 1(b). To quantify the observed variations, we have extracted relaxation rate from the ISF (described in SI[32]) by modeling the ISF with eqn. 2 with relaxation time, τ and Kohlrausch exponent, β as fit parameters. The relaxation rate (Γ) as obtained for PS50k based samples is summarized in Fig. 2. Data for PS100k based samples is shown in Fig. S9. Figure 2(a) shows the wave vector dependent relaxation rate for neat PS films (PS50k) for different temperatures. As expected for a normal viscous melt, the dynamics becomes faster with increasing temperature[39,42]. The wave vector dependence is suggestive of capillary wave dynamics and we have used the well established formalism[42–44] to extract viscosity from such data using the eqn. 3. At this point we woulk like to mention that we did not observe significant difference between the dynamics in the surface and bulk of the films (Fig. SI10), unlike some earlier reports[48]. Hence we have only presented the surface dynamics data. It is possible that this difference with some earlier reports is related to the thickness of the interface adsorbed layer which is estimated to be $\approx 2-3$ nm in our case (Fig. S10c) while it is ≈ 7 nm in the work by Koga et.al[48].

Using the well known temperature dependent γ values for PS[50,51], we have extracted the viscosity, η, for all samples at the corresponding temperatures. Extracted values of viscosity for PS

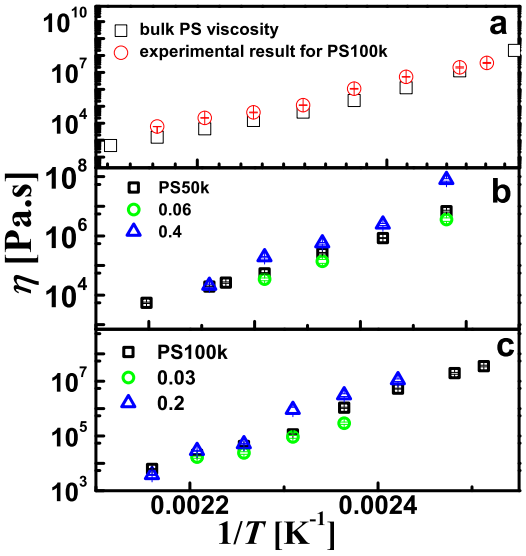

Fig. 3 (a) The comparison of the viscosity estimated for PS100k films and literature values of PS94k bulk viscosity[52]. The Comparison of extracted viscosity, η, from capillary wave fit (eqn. 3) for PS50k matrix based (b) and PS100k matrix based PNCs (c) as a function of T for various values of f. The reduction in η is evident for smaller f and comparatively larger viscosity for higher f.

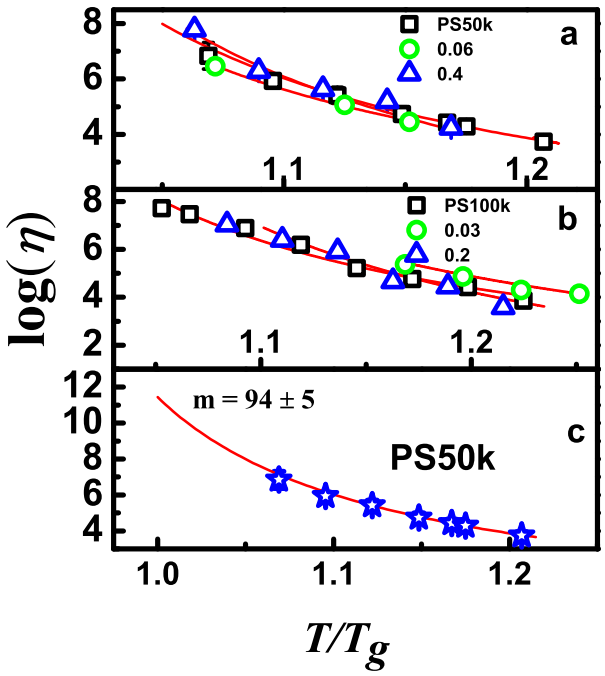

Fig. 4 The viscosity as a function of T/T_g for PS50k (a) and PS100k (b) based samples are shown along with the VFT fits (solid red lines) and, (c) a typical extrapolation of the VFT fit from which the slope near T_g (T/T_g = 1) is calculated to determine the fragility, m.

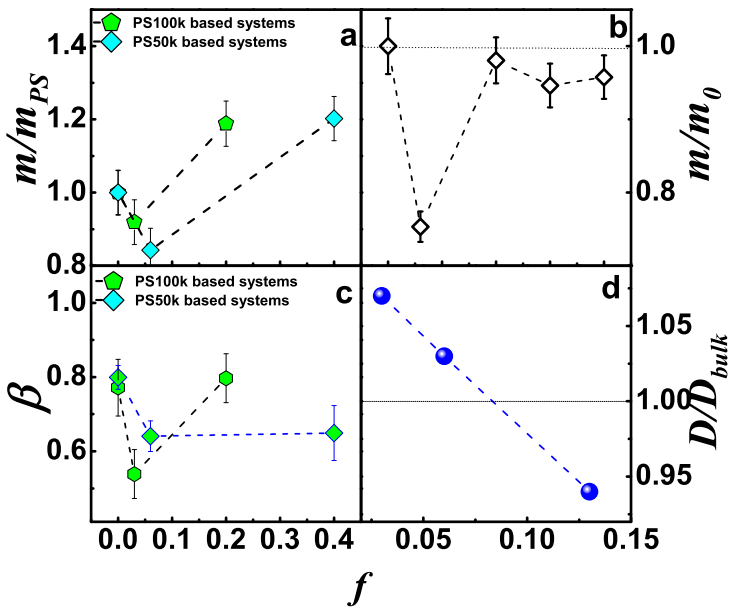

Fig. 5 (a) Estimated fragility, m normalized by m_{PS}, fragility of pure PS films as a function of entropic compatibility, f, from the temperature dependent viscosity is summarized, (b) Fragility, estimated from MD simulation, normalized with that of pure polymer system (m_0) as a function of f showing a clear reduction in m for smaller f, (c) Kohlrausch exponent as a function of f (at $q_x = 7 \times 10^{-4}$ Å^{-1} and averaged over all the temperatures) showing a trend similar to that of m and (d) Diffusivity of polymer chains near the nanoparticle surface, D, normalized to chain diffusivity far away from this interface, D_{blk} as obtained from MD simulation.

films agrees well with the literature values of corresponding bulk PS viscosity as a function of temperature as can be seen in Fig. 3 (a)[52]. The validation of this technique of estimating film viscosity has been well established by several groups[42,53]. The viscosity obtained from XPCS has been found to be in good agreement with the bulk PS viscosity up to a very high molecular weight[44]. In addition, XPCS provides information about dynamic heterogeneity, length scale dependent dynamics and structural variations underlying the dynamics in an integrated manner. Therefore, XPCS is a technique of choice at this stage to acquire all related film information.

Figure 3(b-c) summarize the temperature dependent viscosity behavior for all the samples. For both PS50k (Fig. 3(b)) and PS100k (Fig. 3(c)) based mixtures, it can be observed that the η of PNCs with smaller f is comparably lower than the neat polymers, while the samples with higher f show a slight increase in η. Such reduction in the viscosity of PNC was observed earlier[9,54–57] and alluded to the presence of thin interface layer surrounding the nanoparticles with reduced surface viscosity[9,54] Our earlier observations[39] also indicated the presence of an IL with reduced viscosity compared to the bulk. To quantify the temperature dependence of the observed viscosity, we have modeled the viscosity plots with VFT equation as given in eqn. 4 . The fragility, m, is calculated using eqn. 5. T_g of the films used for the fragility estimation is estimated from AFM force-distance spectroscopy (Fig. S13). Since normal calorimetric methods like differential scanning calorimetry (DSC) can not be used for this films, we have employed this technique which has been well established earlier by ourselves and others[33,58–60] and found reliable to estimate T_g for this type of ultra-thin films. A comparison of T_gs estimated from AFM and that from differential scanning calorimetry (DSC) on several films are shown in table S4 in SI[32]. This suggest that the T_g obtained from AFM is quite reliable.

4 Discussion

Figure 4(a-b) shows the viscosity of all PS50k and PS100k based samples as a function of T/T_g with corresponding VFT fits. In order to obtain the fragility, we have extrapolated this fit till T/T_g = 1 and taken the slope at that point which is demonstrated in Fig. 4(c) for pure PS50k data. Figure 5(a) summarizes the observed variation of m, normalized with that of corresponding pristine polymers (m_{PS}), with f. The fragility (within the error bars[32]) shows an overall trend of lower values at lower f, which rises to values comparable to or even higher than the pristine PS at larger f.

Corroborating most reports, our experiments (Fig. S13) suggest a direct correlation between the changes in T_g and m[25,61]. However, it must be highlighted that the extent of fragility change is much more significant than that of corresponding change in T_g. This signifies that there could be an additional effect of the entropic interaction parameter f on the fragility.

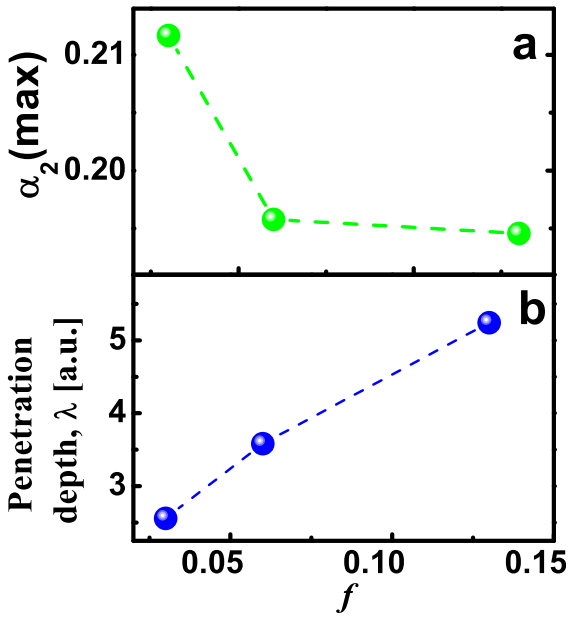

Fig. 6 (a) The peak value of Non-Gaussian Parameter, $\alpha_2(max)$ as a function of f. (b) Penetration depth as a function of f

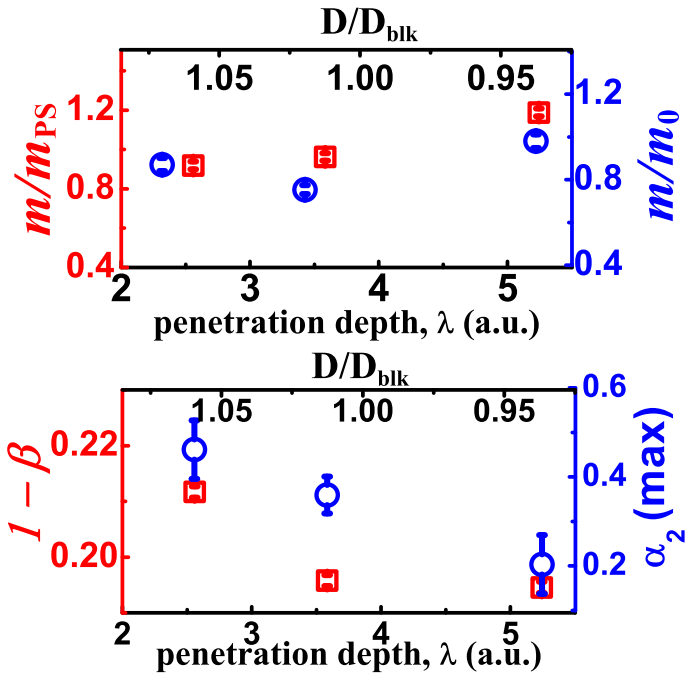

Fig. 7 (a) Master curve showing fragility estimated from experiment (m/m_{PS}) as well as simulation (m/m_0), and (b) (1-β) and $\alpha_2(max)$ as a function of λ and normalized IL diffusivity (D/D$_{blk}$).

In order to obtain microscopic insight on the effect of f on m, we have estimated η of a system with linear polymer chains embedded with grafted nanoparticles, which is similar to the experimental system using MD simulation following established methods[62]. Here grafted chain length was varied keeping matrix same to get a range of f values[32]. The temperature dependent viscosity obtained from these simulations (Fig. S16) has been used for calculating fragility as shown in Fig. 5(b). Interestingly, m/m_0 shows a significant reduction at small f as observed experimentally for our systems (Fig. 5(a)). At larger f, m increases similar to our experimental observations although it does not exceed the value of pure PS. Thus a fairly good qualitative correlation between the experimental and simulation results for fragility is observed.

Thus our observation suggest that entropic PNC[32] with PGNP can show a reduction as well as enhanced fragility by just changing the entropic interaction parameter, f, without changing any direct nanoparticle-polymer or nanoparticle-nanoparticle interaction. In addition, Fig. 5(c) shows the variation of the average, β for various values of f. The variation in β with f looks very similar to that of m. Usually, the smaller the value of β larger is the heterogeneity in dynamics and in such cases, conventionally, the glass former has been identified as also being more fragile. However, in our case, we find that there is an intriguing anti-correlation.

Since the dynamics or viscosity in polymer nanocomposites is essentially determined by the PGNP-matrix IL, we explored the diffusivity of matrix chains in this region for various values of f from MD simulations (Table S5). To do so, we setup a system consisting of a single PGNP, with varied graft length for different f, fixed at the center of simulation box and surrounded by polymer chains. The interface and bulk region is demarcated using the matrix and graft monomer radial density profiles (Fig. S19). As we see from Fig 5(d), normalized (to bulk) IL diffusivity is enhanced at smaller f and progressively reduces at larger f. This indicates that the interfacial diffusivity and fragility are inversely correlated. It is widely believed that for such entropic PNCs, smaller f corresponds to a dewetting nanoparticle polymer interface[11,18,63] with attractive entropic interactions. As the interface becomes wetting (repulsive entropic interactions) by increasing f, the interface diffusivity reduces. Interestingly, the smaller value of β corresponds to larger diffusivity (smaller IL width) and vice versa suggesting that, larger interfacial chain diffusivity could be related to a larger DH (i.e. smaller β). Therefore, these results suggests that the modified IL dynamics at the PGNP-PS interface is crucial in determining various dynamical parameters in these PNCs. To obtain further insight into the DH of the system and its relation with interfacial diffusivity as well as fragility, we have calculated non-gaussian parameter (NGP), α_2, from MD simulation. The peak value of the NGP, $\alpha_2(max)$ (Fig. S23), for several values of f, are summarized in Fig. 6(a). It is quite evident that, $\alpha_2(max)$ decreases with increasing f. Existing reports have established a direct correlation between $\alpha_2(max)$ and DH of the liquid[31,64]. Therefore, the reduction in $\alpha_2(max)$ indicates a decrease in DH in the system with increasing f.

Since f is not a microscopic parameter, we calculated the penetration depth, λ (eqn. 7 of SI) of the matrix chains into grafted brush as function of f which is shown in Fig. 6(b)[65]. It clearly shows a proportionality between λ and f. We use this proportionality of λ and f to depict in Fig. 7 (a,b) the microscopic

correlation of m, β and $\alpha_2(max)$ with λ and D/D_{blk}. While λ and D/D_{blk} has been obtained from MD simulation, and is difficult to extract in experiments, systematic trends are obtained for m and DH in both simulations and experiments. While fragility, increases with λ and D/D_{blk}, DH represented by $1-\beta$, in experiments and $\alpha_2(max)$ in simulations decreases correspondingly. Hence, it is reasonable to conclude that IL microscopic parameters (quantified by λ and D/D_{blk}) plays a considerable role in tuning the m and DH of the PNC system. Importantly, our results suggest an anti-correlation between fragility and dynamical heterogeneity, which is contrary to most recent reports in other types of glasses or PNCs[7,30]. These results also points to the predominance of kinetic fragility in our entropic PNC systems which was alluded to occur in some amorphous polymers earlier[31] but has not been observed in most other PNC systems.

5 Conclusion

In conclusion, we have studied the influence of nanoparticle-polymer interfacial layer dynamics on the fragility and DH of athermal PNC melts. The fragility of PNCs was found to increase with increasing entropic compatibility both in experiments and simulations. The DH on the other hand seemed to decrease with increasing f suggesting an anti-correlation between fragility and DH, contrary to most earlier observations on glasses and polymers. A larger diffusivity of polymer chains was observed at the IL for smaller f, from simulations, which reduces with increasing f and seems to drive the observed dynamical behavior. Finally, the extent of entropic interactions, as determined by λ, tunes the variation of both m and DH. Our work illustrates the subtle correlations between interfacial layer dynamics and dynamical parameters of PNCs, which are critical in determining their flow and mechanical properties.

Conflicts of interest

There are no conflicts to declare.

Acknowledgements

Authors would like to thank the Department of Science and Technology (DST), India for the financial support for facilitating experiments at the P10 beamline in PETRA-III, DESY, Hamburg, Germany.

Notes and references

1 S. Y. Kim and C. F. Zukoski, *Soft Matter*, 2012, **8**, 1801–1810.
2 B. Cappella and D. Silbernagl, *Thin Solid Films*, 2008, **516**, 1952–1960.
3 M. R. Bockstaller and E. L. Thomas, *J. Phys. Chem. B*, 2003, **107**, 10017–10024.
4 A. P. Holt, V. Bocharova, S. Cheng, A. M. Kisliuk, B. T. White, T. Saito, D. Uhrig, J. P. Mahalik, R. Kumar, A. E. Imel *et al.*, *ACS nano*, 2016, **10**, 6843–6852.
5 C.-C. Lin, P. J. Griffin, H. Chao, M. J. A. Hore, K. Ohno, N. Clarke, R. A. Riggleman, K. I. Winey and R. J. Composto, *J. Chem. Phys.*, 2017, **146**, 203332.
6 S. Srivastava and J. K. Basu, *Phys. Rev. Lett.*, 2007, **98**, 165701.
7 S. Cheng, B. Carroll, W. Lu, F. Fan, J.-M. Y. Carrillo, H. Martin, A. P. Holt, N.-G. Kang, V. Bocharova, J. W. Mays, B. G. Sumpter, M. Dadmun and A. P. Sokolov, *Macromolecules*, 2017, **50**, 2397–2406.
8 P. Z. Hanakata, J. F. Douglas and F. W. Starr, *Nat. Comm.*, 2014, **5**, year.
9 M. Wang and R. J. Hill, *Soft Matter*, 2009, **5**, 3940–3953.
10 S. Cheng, V. Bocharova, A. Belianinov, S. Xiong, A. Kisliuk, S. Somnath, A. P. Holt, O. S. Ovchinnikova, S. Jesse, H. Martin, T. Etampawala, D. Mark and A. P. Sokolov, *Nano Lett.*, 2016, **16**, 3630–3637.
11 P. F. Green, *Soft Matter*, 2011, **7**, 7914–7926.
12 S. K. Kumar, N. Jouault, B. Benicewicz and T. Neely, *Macromolecules*, 2013, **46**, 3199–3214.
13 V. Ganesan and A. Jayaraman, *Soft Matter*, 2014, **10**, 13–38.
14 M. E. Mackay, A. Tuteja, P. M. Duxbury, C. J. Hawker, B. Van Horn, Z. Guan, G. Chen and R. Krishnan, *Science*, 2006, **311**, 1740–1743.
15 K. J. Johnson, E. Glynos, S.-D. Maroulas, S. Narayanan, G. Sakellariou and P. F. Green, *Macromolecules*, 2017, **50**, 7241–7248.
16 R. Mangal, S. Srivastava and L. A. Archer, *Nat. Comm.*, 2015, **6**, year.
17 S. A. Kim, R. Mangal and L. A. Archer, *Macromolecules*, 2015, **48**, 6280–6293.
18 D. Meng, S. K. Kumar, J. M. D. Lane and G. S. Grest, *Soft Matter*, 2012, **8**, 5002–5010.
19 N. Mauro, M. Blodgett, M. Johnson, A. Vogt and K. Kelton, *Nat. Comm.*, 2014, **5**, year.
20 S. Askar, L. Li and J. M. Torkelson, *Macromolecules*, 2017.
21 D. Cangialosi, A. Alegría and J. Colmenero, *J. Chem. Phys.*, 2006, **124**, 024906.
22 M. Ozawa, K. Kim and K. Miyazaki, *J. Stat. Mech.: Theo. Exp.*, 2016, **2016**, 074002.
23 J. Mattsson, H. M. Wyss, A. Fernandez-Nieves, K. Miyazaki, Z. Hu, D. R. Reichman and D. A. Weitz, *Nature*, 2009, **462**, 83–86.
24 B. A. P. Betancourt, J. F. Douglas and F. W. Starr, *Soft Matter*, 2013, **9**, 241–254.
25 S. Cheng, S.-J. Xie, J.-M. Y. Carrillo, B. Carroll, H. Martin, P.-F. Cao, M. D. Dadmun, B. G. Sumpter, V. N. Novikov, K. S. Schweizer and A. P. Sokolov, *ACS Nano*, 2017, **11**, 752–759.
26 H. Oh and P. F. Green, *Nat. Mat.*, 2009, **8**, 139–143.
27 R. Böhmer, K. Ngai, C. Angell and D. Plazek, *J. Chem. Phys.*, 1993, **99**, 4201–4209.
28 L. Hong, V. N. Novikov and A. P. Sokolov, *J. Non-Crystal. Solids*, 2011, **357**, 351–356.
29 A. Wisitsorasak and P. G. Wolynes, *J. Phys. Chem. B*, 2014, **118**, 7835–7847.
30 T. Sasaki, M. Ichimura and S. Irie, *Polym. J.*, 2015, **47**, 687–694.
31 T. Kanaya, l. Tsukushi and K. Kaji, *Prog. Theor. Phys. Supp.*, 1997, **126**, 133–140.

32 *Supplementary Information*.

33 S. Chandran, N. Begam, V. Padmanabhan and J. K. Basu, *Nat. Comm.*, 2014, **5**, 3697.

34 N. Begam, S. Chandran, N. Biswas and J. K. Basu, *Soft Matter*, 2015, **11**, 1165–1173.

35 M. K. Corbierre, N. S. Cameron, M. Sutton, K. Laaziri and R. B. Lennox, *Langmuir*, 2005, **21**, 6063–6072.

36 W.-S. Jang, P. Koo, K. Bryson, S. Narayanan, A. Sandy, T. P. Russell and S. G. Mochrie, *Macromolecules*, 2014, **47**, 6483–6490.

37 S. Narayanan, D. R. Lee, A. Hagman, X. Li and J. Wang, *Phys. Rev. Lett.*, 2007, **98**, 185506.

38 S. Srivastava, P. Agarwal, R. Mangal, D. L. Koch, S. Narayanan and L. A. Archer, *ACS Macro Lett.*, 2015, **4**, 1149–1153.

39 N. Begam, S. Chandran, M. Sprung and J. K. Basu, *Macromolecules*, 2015, **48**, 6646–6651.

40 A. K. Kandar, S. Srivastava, J. K. Basu, M. K. Mukhopadhyay, S. Seifert and S. Narayanan, *J. Chem. Phys.*, 2009, **130**, 121102.

41 S. Chandran, C. K. Sarika, A. K. Kandar, J. K. Basu, S. Narayanan and A. Sandy, *J. Chem. Phys.*, 2011, **135**, 134901.

42 H. Kim, A. Rühm, L. B. Lurio, J. K. Basu, J. Lal, D. Lumma, S. G. J. Mochrie and S. K. Sinha, *Phys. Rev. Lett.*, 2003, **90**, 068302.

43 Z. Jiang, H. Kim, S. G. Mochrie, L. Lurio and S. K. Sinha, *Phys. Rev. E*, 2006, **74**, 011603.

44 H. Kim, A. Rühm, L. B. Lurio, J. K. Basu, J. Lal, S. G. J. Mochrie and S. K. Sinha, *Phys. B: Cond. Matt.*, 2003, **336**, 211–215.

45 S. G. J. Mochrie, L. B. Lurio, A. Rühm, D. Lumma, M. Borthwick, P. Falus, H. J. Kim, J. K. Basu, J. Lal and S. K. Sinha, *Phys. B: Cond. Matt.*, 2003, **336**, 173–180.

46 B. A. P. Betancourt, P. Z. Hanakata, F. W. Starr and J. F. Douglas, *Proceed. National Acad. Sci.*, 2015, **112**, 2966–2971.

47 V. N. Novikov and A. P. Sokolov, *Nature*, 2004, **431**, 961–963.

48 T. Koga, N. Jiang, P. Gin, M. K. Endoh, S. Narayanan, L. B. Lurio and S. K. Sinha, *Phys. Rev. Lett.*, 2011, **107**, 225901.

49 T. Koga, C. Li, M. K. Endoh, J. Koo, M. Rafailovich, S. Narayanan, D. R. Lee, L. B. Lurio and S. K. Sinha, *Phys. Rev. Lett.*, 2010, **104**, 066101.

50 S. Wu, *J. Phys. Chem.*, 1970, **74**, 632–638.

51 S. Chandran and G. Reiter, *Phys. Rev. Lett.*, 2016, **116**, 088301.

52 D. J. Plazek and V. M. O'Rourke, *Journal of Polymer Science Part A-2: Polymer Physics*, 1971, **9**, 209–243.

53 C. Li, T. Koga, C. Li, J. Jiang, S. Sharma, S. Narayanan, L. B. Lurio, X. Hu, X. Jiao, S. K. Sinha, S. Billet, D. Sosnowik, H. Kim, J. C. Sokolov and M. H. Rafailovich, *Macromolecules*, 2005, **38**, 5144–5151.

54 F. Chen, D. Peng, Y. Ogata, K. Tanaka, Z. Yang, Y. Fujii, N. Yamada, C.-H. Lam and O. K. Tsui, *Macromolecules*, 2015, **48**, 7719–7726.

55 K. Nusser, G. J. Schneider, W. Pyckhout-Hintzen and D. Richter, *Macromolecules*, 2011, **44**, 7820–7830.

56 H. Goldansaz, F. Goharpey, F. Afshar-Taromi, I. Kim, F. J. Stadler, E. van Ruymbeke and V. Karimkhani, *Macromolecules*, 2015, **48**, 3368–3375.

57 M. E. Mackay, T. T. Dao, A. Tuteja, D. L. Ho, B. Van Horn, H.-C. Kim and C. J. Hawker, *Nature materials*, 2003, **2**, 762.

58 N. Delorme, M. S. Chebil, G. Vignaud, V. Le Houerou, J.-F. Bardeau, R. Busselez, A. Gibaud and Y. Grohens, *Euro. Phys. J. E*, 2015, **38**, 56.

59 B. Cappella, S. K. Kaliappan and H. Sturm, *Macromolecules*, 2005, **38**, 1874–1881.

60 R. Mangal, S. Srivastava, S. Narayanan and L. A. Archer, *Langmuir*, 2016, **32**, 596–603.

61 P. Z. Hanakata, B. A. Pazmiño Betancourt, J. F. Douglas and F. W. Starr, *J. Chem. Phys.*, 2015, **142**, 234907.

62 V. Padmanabhan, *J. Chem. Phys.*, 2012, **137**, 094907.

63 B. Palli and V. Padmanabhan, *Soft matter*, 2014, **10**, 6777–6782.

64 C. Bennemann, C. Donati, J. Baschnagel and S. C. Glotzer, *Nature*, 1999, **399**, 246–249.

65 M. Ibrahim, N. Begam, V. Padmanabhan and J. K. Basu, *Soft matter*, 2018, **14**, 6076–6082.